RSC Advances

Fe/amorphous SnO2 core-shell structured nanocapsules for microwave absorptive and electrochemical performance

Journal:	*RSC Advances*
Manuscript ID:	RA-ART-08-2014-008998.R2
Article Type:	Paper
Date Submitted by the Author:	01-Oct-2014
Complete List of Authors:	Liu, Xianguo; Institute of Metal Research, Shenyang National Laboratory for Material Science Zhou, Guiping; Electric Power Research Institute of State Grid Liaoning Electric Power Co., Ltd., Or, Siu Wing; The Hong Kong Polytechnic University, Department of Electrical Engineering Sun, Yuping; Center for Engineering practice and Innovation Education, Anhui University of technology

Cite this: DOI: 10.1039/c0xx00000x

www.rsc.org/advances

PAPER

Fe/amorphous SnO_2 core-shell structured nanocapsules for microwave absorptive and electrochemical performance

Xianguo Liu,*[a,b] Guiping Zhou,[c] Siu Wing Or,*[b] and Yuping Sun[a]

Received (in XXX, XXX) Xth XXXXXXXXX 20XX, Accepted Xth XXXXXXXXX 20XX

DOI: 10.1039/b000000x

Fe nanocapsules with Fe nanoparicles core and amorphous SnO_2 shell have been synthesized by the modified arc discharge method. The microwave absorption properties and electrochemical performances of Fe/amorphous SnO_2 nanocapsules were investigated. The synergistic effect of magnetic loss in Fe nanoparticles core and dielectric loss in SnO_2 shell made the Fe/SnO_2 nanocapsules with the excellent microwave absorption properties. Reflection loss (RL) values of Fe/SnO_2 nanocapsules-paraffin composite is -39.2 dB at 16.8 GHz at the absorbent thickness of 2 mm and the absorption bandwidth with the RL below -20 dB is up to 10.6 GHz (from 7.4 to 18 GHz) for the absorber with the thickness in 2 - 3.8 mm. When evaluated as anode materials for lithium-ion batteries, the Fe/amorphous SnO_2 nanocapsules deliver an initial discharge of 1558.7 mAh g^{-1} at 38 mA g^{-1} and maintain a reversible capacity of 698.2 mAh g^{-1} over 100 cycles, which is attributed to the amorphous SnO_2 nanoshell.

1. Introduction

In the past decades, nanocomposites consisting of transition metals and semiconductor materials, especially those with core-shell structures, have drawn growing interests owing to their unique structural features and unusual properties that endow them with great potential for various applications, such as microwave absorbers and lithium-ion batteries (LIBs).[1-5] Microwave absorber is a kind of functional material that can absorb electromagnetic (EM) wave effectively and convert EM energy into thermal energy or make EM wave dissipate by interference.[6-8] The serious EM pollution/radiation and shielding interference in the field of electric communication result in the increasing demand for the development of novel high-efficient microwave absorbers with light density, low cost, thin thickness, wide absorption frequency range, and strong absorption abilities .[9] Recently, core-shell structured nanocapsules have been subject to extensive study for the combined functionalities of cores and shells that show great potential for broadband lightweight absorbers with lower reflection loss than single-component microwave absorbers .[1-4,6-8] Due to the high saturation magnetization, high initial permeability, high Curie temperature of iron, the previous work mainly studied the effect of various Fe-based nanocapsules with dielectric shells on the microwave absorption performances.[10-14] Fe-based nanocapsules with the semiconductor shells have been rarely focused on. Fe-based nanocapsules with the semiconductor shells possess the combined effect of excellent magnetic properties of Fe cores and the high resistivity of semiconductors, which ensures their excellent microwave absorption properties .[4,15]

Recently, global warming, diminishing fossil-fuel supplies, and environmental pollution have driven the increasing usage of rechargeable LIBs. To apply LIBs in electric vehicles and renewable energy storage, a significant advance in energy storage density, power density, and cycle life is required.[16-18] Tremendous efforts have been focused on developing alternative high performance electrode materials for next generation LIBs, especially metal oxides due to their high theoretical capacitance, natural abundance and low cost.[19-23] Among numerous new candidates of anode materials, SnO_2, an important *n*-type semiconductor (*Eg*=3.6 eV), has been considered as promising negative electrode materials due to its high theoretical capacity (782 mAh g^{-1}).[24] However, the significant disadvantages of SnO_2 are the poor cyclability due to the large volume expansion (~300 %) during the discharge/charge processes and the high irreversible capacity loss from the formation of Li_2O.[21] As one of the effective ways, nanostructured SnO_2 such as 1D nanowires,[25] 2D nanosheets,[26] and 3D porous nanostructures,[27] will be more able to withstand the huge volume change during the charge-discharge process. Furthermore, it has been reported that introducing core-shell structured nanocomposites is a new way to activate the irreversible capacity of alloy-type metal oxide because the metal nanoparticles in the cores can make extra Li_2O reversibly converting to Li^+.[28] However, few amorphous nanostructured SnO_2 are reported as the anode materials for LIBs. Amorphous electrodes show better cycling characteristics than crystalline electrodes, primarily due to the continuous and single-phase reaction without phase transformation and with more homogeneous volume expansions.[29] A further advantage is the relatively fast Li transport in the amorphous phase.[30] More importantly, electrodes remain fully amorphous during lithiation/delithiation cycling, avoiding problems associated with crystalline-amorphous phase transitions.[22] In the present work, Fe/amorphous SnO_2 core-shell structured nanocapsules have been synthesized by the arc discharge technique. A combination of a

magnetic core and a semiconductor shell would widen the application of this kind of multi-functional nanocapsules. The microstructures, magnetic properties, EM properties and electrochemical performances of Fe/SnO_2 nanocapsules are investigated systematically and the effects of the core-shell microstructure are discussed in detail.

2. Experimental

2.1 Synthesis of Fe/amorphous SnO_2 core-shell structured nanocapsules

In this work, the Fe/amorphous SnO_2 core-shell structured nanocapsules were fabricated by the modified arc-discharge method, which was described in detail in our previous work .[2,12,15] According to the Wang's report,[31] Fe-Sn alloy or Sn appear when the Sn content of the used Fe-Sn target is over 2 at%. Micrometer powders of metallic Fe and Sn of 99% purity were well mixed for the preparation of $Fe_{99}Sn$ (at.%) target. In brief, $Fe_{99}Sn$ target served as the anode, while the cathode was a tungsten needle. The anode target was placed into a water-cooled copper crucible. After the chamber was evacuated (in a vacuum of 1.0×10^{-2} Pa), argon gas of 1.6×10^{4} Pa was introduced into the chamber. The arc-discharge current was maintained at 40 A for 1 h to evaporate the target sufficiently. Then the product in the form of powder was collected from material deposited at the top of the water-cooled chamber, after passivated for 24 h in air.

2.2 Materials characterizations

The phase analysis for the product was performed by using powder X-ray diffraction (XRD), acquired by a Bruker D8 Advance X-ray diffractometer equipped with a monochromatized Cu-Kα radiation. The morphology and size distribution of the products were observed by a high-resolution transmission electron microscope (HRTEM) images from JEOL-2100F. Magnetization measurements were carried out using a vibration sample magnetometer (VSM). The surface composition was analyzed by an X-ray photoelectron spectroscopy (XPS) spectrometer, using Mg Kα line (1253.6 eV) excitation (Perkin Elmer PHI 1600 ESCA system).

2.3 Electromagnetic absorbing measurement

The Fe/SnO_2 nanocapsules-paraffin composite was prepared by uniformly mixing Fe/SnO_2 nanocapsules with paraffin, and the detailed descriptions can be found elsewhere.[2, 6, 10, 12-15] The mixture was compressed into a cylinder-shaped compact, and then cut into a toroidal shape with 7.00 mm outer diameter and 3.04 mm inner diameter. The EM parameters of Fe/SnO_2 nanocapsule (40 wt.%)-paraffin composites were measured using an Agilent N5244A vector network analyzer (VNA, USA). Coaxial method is used to determine the EM parameters of the toroidal samples in the frequency range of 2-18 GHz in transverse EM mode. The vector network analyzer was calibrated for the full two-port measurement of reflection and transmission at each port. The complex permittivity ($\varepsilon_\gamma=\varepsilon'-j\varepsilon''$) and complex permeability ($\mu_\gamma=\mu'-j\mu''$) were calculated from S-parameters using a simulation program of Reflection/Transmission Nicolson-Ross model.[2, 6, 10, 12-15]

2.4 Electrochemical tests

The electrodes were fabricated by mixing the Fe/SnO_2 nanocapsules, ketjen black and polyvinylidene difluoride (PVDF) at a weight ratio of 70:20:10. A slurry was prepared by thoroughly mixing an N-methyl-2-pyrrolidone solution of PVDF, Fe/SnO_2 nanocapsules and ketjen black, which was then coated on copper foil and dried in a vacuum baking oven at 120 ^{o}C for 10 hours. The coin-type cells (CR2016) were assembled in an argon filled glove box. Celgard 2325 was used as the separator. Pure lithium disks were used as the counter and reference electrodes. The electrolyte was 1 M LiPF6 in ethylene carbonate (EC): dimethyl carbonate (DMC) (1:1 in volume). Charge/discharge cycling was performed on the PAR2273 Electrochemical Measurement System (EG&G Princeton Applied Research) at 0.01-2.5 V. A cyclic voltammetric (CV) measurement of the electrode was cycled by Land 2001A with a scan rate of 0.1 mV s^{-1} at room temperature.

3. Results and Discussion

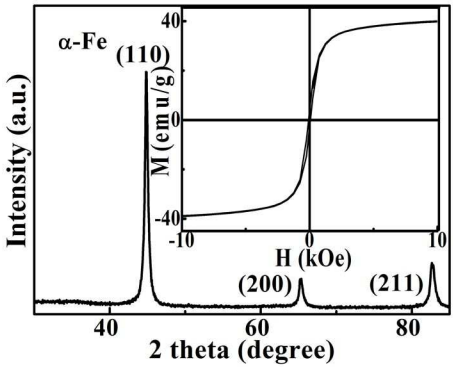

Fig. 1 XRD pattern of α-Fe/SnO_2 nanocapsules. The inset is the magnetic hysteresis loop at 295 K.

The XRD pattern is shown in Fig.1, indicating that all sharp reflections can be indexed with the body-centered cubic α-Fe phase (JCPDS card No. 87-0722) with lattice parameter of a = 2.860 Å. The average grain size of α-Fe is calculated to be about 18 nm from the full width at half maximum of the Fe (110) Bragg scatting peak intensity using Debye-Scherrer's formula: $D=(0.89\lambda)/[\delta(2\theta)\cos\theta)]$, where λ is the X-ray wavelength, $\delta(2\theta)$ the line broadening at half of the maximum intensity in radians, and θ the Bragg scattering angle. However, in the present case, the Sn-oxide shells are not detected by XRD, because probably only a small amount of Sn-oxides is present on the shell of the nanocapsules, and also due to the amorphous nature and the lack of the translational symmetry of the shell. The inset of Fig.1 shows the hysteresis loop of the α-Fe/SnO_2 nanocapsules at 295 K. The saturation magnetization of the α-Fe/SnO_2 nancapsules reaches 39.9 emu/g, which is 19 % of the bulk α-Fe value. This difference in the bulk property is explained by weakly coupled and more disordered spins on the surface and the existence of a nonmagnetic SnO_2 component.[15]

A TEM image in Fig. 2(a) shows a group of α-Fe/SnO_2 nanocapsules. The nanocapsules are nearly spherical in shape with a diameter distribution of 30-50 nm. The HRTEM image, as

shown in Fig. 2(b), clearly indicates that the nanocapsules own a 'core/shell' type structure and inner α-Fe nanoparticles core are encapsulated into the amorphous shell with the thickness of 7 nm. In order to obtain more information on amorphous shell, we investigated α-Fe/SnO_2 nanocapsules with XPS at an etching depth of 1 nm. As shown in Fig.2(c), the binding energy peaks of Sn 3d3/2 and Sn 3d5/2 for the Fe/SnO_2 nanocapsules are 495.36 eV and 487.10 eV, respectively, indicating the shell is thicker than 1 nm. Because 487.10 eV and 495.36 eV are consistent with the binding energy of Sn 3d5/2 and Sn3d3/2 in SnO_2,[32, 33] the shells of nanocapsules can be identified as SnO_2. The formation mechanism of the Fe/SnO_2 nanocapsules can be ascribed to the different evaporating pressures and melting points for Fe and Sn atoms during the arc discharging process. When the temperature is decreased, the Fe atoms with higher melting point first form a nucleus and these Sn atoms with lower melting point are abundant on the surfaces of the Fe nanoparticles. When the products are passivated in air, Sn atoms are easily oxidized to amorphous SnO_2 on the surfaces of the nanocapsules to form the core/shell structure.[15]

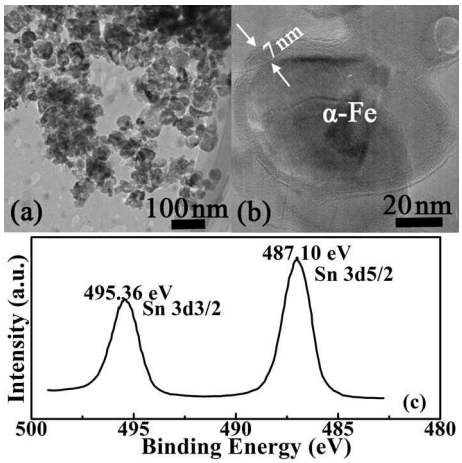

Fig. 2 (a) TEM image and (b) HRTEM image of α-Fe/SnO_2 nanocapsules; (c) XPS spectrum of the Sn 3d electrons on the surface with an etching depth of 1 nm.

The microwave absorption properties of the Fe/SnO_2 nanocapsules are determined by the relative complex permeability (μ_γ) and permittivity (ε_γ) at a given frequency and layer thickness. The real parts and imaginary parts of EM parameters correspond to the energy storage and loss of EM waves in the propagation process .[6] Fig.3(a) shows the frequency dependence of the real part (ε') and the imaginary part (ε'') of ε_γ of the Fe/SnO_2-paraffin composites in the 2-18 GHz range. The ε' of the composite declines from 11.26 to 5.2 in the frequency range of 2-18 GHz. The dielectric performance of the material depends on ionic, electronic, orientational, and space charge polarization .[1] The space charge polarization appears due to the heterogeneity of the nanocapsules and the orientational polarization is raised by bound charges (dipoles).[1, 7] As the frequency of the EM field is increased, the dipoles could not reorient themselves fast enough to respond to an applied electric field, thus the dielectric constant decreases.[1, 7] Maximum/minimum values can be found below/above the resonant frequencies in the ε' curve. Accordingly, two typical dielectric resonances at 3.8 and 16 GHz are obviously observed in the ε'' curve, indicating that they are from the synthetic effect of the Fe nanoparticles cores and SnO_2 shells. The peak at around 14 GHz may be from the spin wave excitations.[13] The Fe/SnO_2 nanocapsules not only present an enhanced dielectric behavior but also combine with the magnetic resonance behavior of Fe nanoparticles. The real part (μ') and imaginary part (μ'') of μ_γ of the Fe/SnO_2-paraffin composites are presented in Fig. 3(b). The μ' values decrease with increasing frequency. At around 3 GHz, the μ' curve implies a normal resonance. Meanwhile, the μ'' values show a peak at 3.2 GHz, which implies that the natural resonance occurs in the Fe/SnO_2 nanocapsules. The natural resonance at 3.2 GHz frequency range is due to the small size effect, the surface effect and spin wave excitations,[1] which is important for their use as microwave absorption materials in the GHz frequency region. The real parts and imaginary parts of EM parameters correspond to the energy storage and loss of EM waves in the propagation process, respectively.[6] The loss capacities can be simplified by dielectric loss factor ($\tan\delta_M=\varepsilon''/\varepsilon'$) and magnetic loss factor ($\tan\delta_M=\mu''/\mu'$), which are shown in Fig.3(c). Both the dielectric loss factor and magnetic loss factor exhibit a broad peak at 2-6 GHz. It is thought that the dielectric loss factor and magnetic loss factor are mutually exclusive and difficult to be simultaneously enhanced for single-component materials.[6] For the absorbers, high-performance microwave absorption mainly results from proper EM impedance matching. A delta-function method has been put forward to effectively evaluate the EM impedance matching degree.[34] The smaller delta value implies better EM impedance matching. The delta values, smaller than 0.2, correspond to the RL below -8 dB.[34] Based on the method proposed in ref. 34, the calculated delta value map of the Fe/SnO_2 nanocapsules is shown in Fig.3(d). The dark blue area indicates the excellent microwave absorption properties.

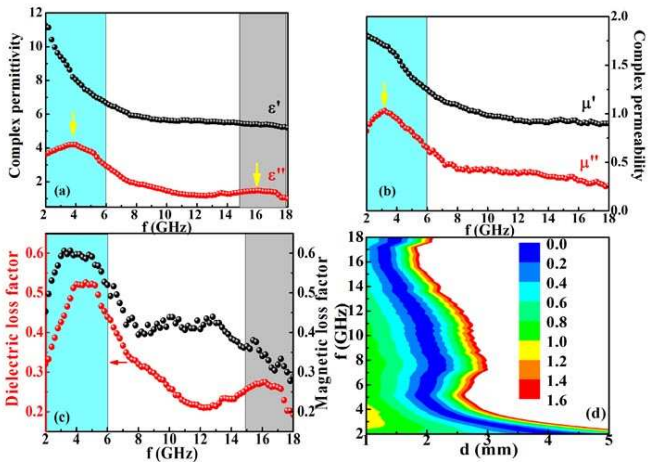

Fig. 3 (a) complex permittivity and (b) complex permeability and (c) magnetic loss factor and dielectric loss factor and (d) calculated delta value map of Fe/SnO_2 nanocapsules.

Therefore, the core/shell structured Fe/SnO_2 nanocapsules should have excellent EM absorption properties, due to the effect

of dielectric resonances and magnetic resonances. According to the transmit-line theory, the reflection loss (RL) can be calculated by the following equations:

$$Z_{in} = Z_0(\mu_r/\varepsilon_r)^{1/2}\tanh[j(2\pi fd/c)(\mu_r\varepsilon_r)^{1/2}]$$
$$RL = 20\lg|(Z_{in}-Z_0)/(Z_{in}+Z_0)| \quad (1)$$

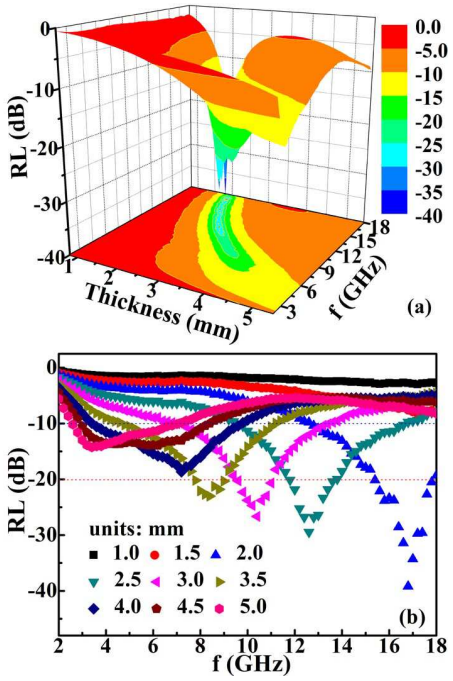

Fig.4 (a) Three-dimensional (3D) representation of the RL derived from the measured ε_γ and μ_γ of the Fe/SnO_2-paraffin composite as a function of the frequency. (b) RL of the Fe/SnO_2-paraffin composite with the thickness range from 1.0 to 5.0 mm.

Where Z_{in} is the input impedance of the absorber, μ_r and ε_r are, respectively, the relative complex permeability and permittivity, c is the velocity of electromagnetic waves in free space, f is the frequency of microwaves, and d is the thickness of the absorber. The RL of the Fe/SnO_2 nanocapsules with the thickness of the absorber varied from 0.8 to 5.4 mm can be calculated as shown in Fig. 4. From the RL curves in Fig.4(a), we can get the following properties: (1) the optimal RL obviously shifts to the lower frequency range with increasing thickness of the layer; (2) the RL peak intensity first increases then decreases with the increase of the thickness; and (3) the RL peak intensity almost keeps a constant when the thickness is thicker than 4.5 mm. Tao et al introduced the model of an EM wave normally incident on an absorber without and with a backed metal plate to explain the absorbing mechanism.[35] Through analyzing and calculating the energy of the EM waves reflected from the air-absorber and absorber-metal plate interfaces, it was concluded that the intensity of the RL peak is determined by the energy difference of the two waves. When the energy of the two reflected waves is equal, the intensity of the RL peak is strongest, otherwise it becomes weak.[35] According to the electromagnetic loss model, the peak of both dielectric loss and magnetic loss are useful to significantly absorb the electromagnetic wave energy. Hence, the absorbing peak should be at 2-6 GHz and keep at 2-6 GHz. However, the simulated results show that the RL peak frequency is closely related to the thickness. Tao et al introduced the quarter-wavelength condition ($d=nc/4f(\varepsilon_\gamma\mu_\gamma)^{1/2}$, (n=1,3,5…)) to well explain the phenomena.[35] As shown in Fig. 4(b), it indicates that the maximum RL reaches -39.2 dB at 16.8 GHz for the absorber with the thickness in 2 mm. Moreover, the absorption bandwidth with the RL below -20 dB covers 10.6 GHz (from 7.4 to 18 GHz) for the absorber with the thickness in 2 - 3.8 mm. Compared with the FeCo/C/polyaniline, Fe/TiO_2, FeCo/Al_2O_3, Fe_3O_4/Au, Fe/SnO, Ni/SiO_2, FeCo/C, Ni/grapheme, Fe/C naomaterials,[1,2,4-6,9-15] the bandwidth and thickness of Fe/SnO_2 nanocapsules with RL below -20 dB is wide and thin, respectively. The special core/shell microstructure of the present nanocapsules with amorphous SnO_2 shells and Fe nanoparticles cores is vital for the excellent EM absorption properties, including strong absorption abilities and wide band absorption.

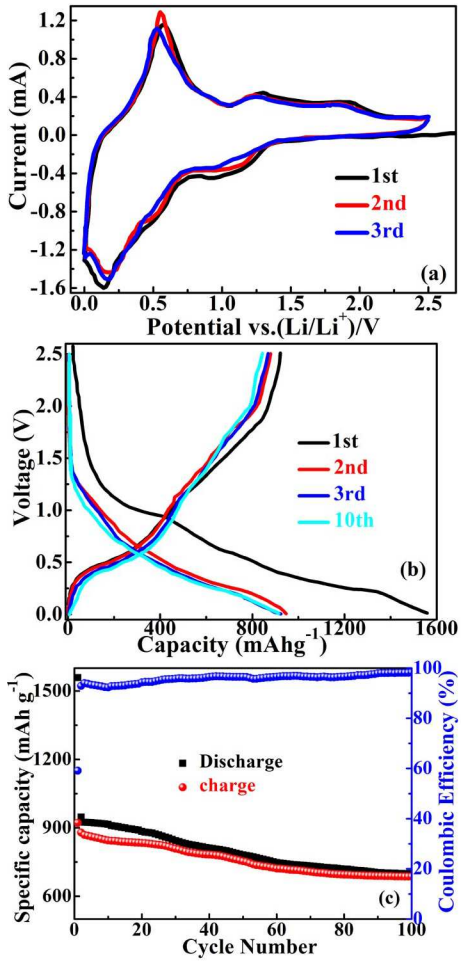

Fig.5 (a) CV curves of Fe/SnO_2 nanocapsules for the first three cycles, with scanning rate of 0.1 mV s^{-1}. (b) Charge-discharge profiles of the Fe/SnO_2 nanocapsules in the initial three cycles and the 10th cycle at a current of 38 mA g^{-1}. (c) The cycling performance at a current of 38 mA g^{-1}, and cycle number vs coulombic efficiency plots of Fe/SnO_2 nanocapsules electrode.

The as-prepared Fe/amorphous SnO_2 core-shell structured nanocapsules were further investigated as a potential anode for LIBs. Cyclic voltammogram (CV) was used to estimate electrochemical process of the Fe/SnO_2 nanocapsules. The first three CV curves of Fe/SnO_2 nanocapsules electrode at a scan rate of 0.1 mV s^{-1} in the potential window of 0.01- 2.5 V (versus Li/Li^+) were characterized, as displayed in Fig.5(a). As can be seen, the curves of these curves are in good agreement with the electrochemical behavior of SnO_2-based anodes as described previously:[21,36]

$$Li^+ + e^- + \text{electrolyte} \rightarrow \text{SEI layer} \quad (2)$$

$$SnO_2 + 4Li^+ + 4e^- \rightarrow Sn + 2Li_2O \quad (3)$$

$$Sn + xLi^+ + xe^- \rightarrow Li_xSn \ (0 \le x \le 4.4) \quad (4)$$

In the initial CV cycle, a broad reduction peak between 0.84 V and 1.36 V is attributed to the lithium insertion to SnO_2 to form Sn and Li_2O, accompanied by the decomposition of electrolyte to form a solid electrolyte interphase (SEI) layer (Eq.(2)).[21] Lithium ions subsequently insert to Sn to form Li_xSn ($0 \le x \le 4.4$) compounds, down to the cut-off voltage of 0.01 V. During the anodic scanning, there are three oxidation peaks presented at around 0.56, 1.26 and 1.86 V, corresponding to the oxidation stages of lithium ions extracted from Li_xSn alloy (Eq.(4)) and partly reversible reaction from Sn to SnO_2 (Eq.(3)), respectively consistent with the results previously described.[21,36,37] The CV curves of the second and third cycles are identical, indicating an excellent reversibility of the Fe/SnO_2 electrode.

The discharge and charge curves for the first three and 10th cycles as shown in Fig.5(b), the discharge and charge current density is 38 mA g^{-1} (corresponding to 0.05 C). The initial discharge and charge capacities are 1558.7 and 921.8 mAh g^{-1}, respectively. The initial capacity loss can be ascribed to the formation of SEI film and electrolyte decomposition, which are common for most anode materials.[20-37] Despite the large initial loss, the Fe/amorphous SnO_2 nanocapsules electrode exhibits very stable cycling performance under such testing conditions (Fig.5(c)). The discharge capacity slowly decreases to a value of about 698.2 mAh g^{-1} after 100 cycles, which is still significantly higher than the theoretical capacity for graphite (372 mAh g^{-1}). The initial Coulombic efficiency of the Fe/amorphous SnO_2 nanocapsules is about 59.1 % and it keeps steadily more than 94 % since the 20th cycle as shown in Fig.5(c). It is worth mentioning that the capacity retention of these Fe/SnO_2 nanocapsules is significantly enhanced when compared with many other SnO_2 nanostructures because of their unique microstructure.[24, 38-41] The amorphous SnO_2 nanshell could accommodate for the volume expansion, provide more reaction sites on the surface and give channels that could efficiently enable solvated Li^+ transport, which may be responsible for the good performance.

Conclusions

We have synthesized Fe/amorphous SnO_2 core-shell structured nanocapsules by the arc discharge method. The microwave absorption properties of Fe/amorphous nanocapsules have been investigated. RL values of Fe/SnO_2 nanocapsules-paraffin composite is -39.2 dB at 16.8 GHz at the absorbent thickness of 2 mm and the absorption bandwidth with the RL below -20 dB is up to 10.6 GHz (from 7.4 to 18 GHz) for the absorber with the thickness in 2 - 3.8 mm. The excellent microwave absorption performance is ascribed to the synergistic effect of magnetic loss in Fe nanoparticles core and dielectric loss in amorphous SnO_2 shell. As an anode material for LIBs, Fe/amorphous nanocapsules exhibit a high initial capacity of 1558.7 mAh g^{-1} and 698.2 mAh g^{-1} after 100 cycles. The amorphous SnO_2 nanoshells have advantages for short lithium diffusion length and large electrode/electrolyte contact area for volume change during charging/discharging process.

Acknowledgements

This study was supported by the National Natural Science Foundation of China (Grant No. 51201002), the Research Grants Council of the HKSAR Government (Grant No. PolyU 5236/12E), and The Hong Kong Polytechnic University (Grant Nos. G-YK59).

Notes and references

[a]*School of Materials Science and Engineering, Anhui University of Technology, Maanshan,243002, China. Fax:+86 555 2311570; Tel: +86 555 2311570; E-mail: liuxianguohugh@gmail.com*
[b]*Department of Electrical Engineering, The Hong Kong Polytechnic University, Hum Hom, Kowloon, Hong Kong. E-mail: eeswor@polyu.edu.hk*
[c]*Electric Power Research Institute of State Grid Liaoning Electirc Power Co., Ltd., Shenyang 110006, PR China.*
[d]*Center for Engineering practice and Innovation Education, Anhui University of Technology, Maanshan,243032, China.*

† Electronic Supplementary Information (ESI) available: See DOI: 10.1039/b000000x/

1 J.J. Jiang, D. Li, D.Y. Geng, J. An, J. He, W. Liu and Z.D. Zhang, Nanoscale 6 2014, 6, 3967-3971.
2 X.G. Liu, Q.Z. Ou, D.Y. Geng, Z. Han, Z.G. Xie and Z.D. Zhang, J. Phys. D: Appl. Phys. 2009,42, 155004
3 J.W. Liu, J. Cheng, R.C. Che, J.J. Xu, M.M. Liu and Z.W. Liu, J. Phys. Chem. C 2013, 117, 489-495.
4 Q. Zhang, C.F. Li, Y.N. Chen, Z. Han, H. Wang, Z.J. Wang, D.Y. Geng, W. Liu and Z.D. Zhang, Appl. Phys. Lett. 2010, 97, 133115.
5 X.G. Liu, Y.P. Sun, C. Feng, C.G. Jin and F. Xiao, J. Power Sources 2014, 245, 256-261.
6 X.F. Zhang, P.F. Guan and J.J. Guo, Part. Part. Syst. Charact. 2013, 30, 842-846.
7 A. Ohlan, K. Singh, A. Chandra and S.K. Dhawan, ACS Appl. Mater. Interfaces 2010, 2, 927-933.
8 J. Cao, W.Y. Fu, H.B. Yang, Q.J. Yu, Y.Y. Zhang and G.T. Zou, J. Phys. Chem. B 113 2009, 113, 4262-4647.
9 Z.H. Wang, L.W. Jiang, D. Li, J.J. Jiang, S. Ma, H. Wang, D.Y. Geng, J. An, J. He and W. Liu, J. Appl. Phys. 2014, 115, 17A527.
10 L.G. Yan, J.B. Wang, X.G. Liu, J. Li, D.Y. Geng and Z.D. Zhang, Appl. Phys. Lett. 2009, 95, 023114.
11 V. Gupta, M.K. Patra, A. Shukla, L. Saini, S. Songara, R. Jani, S.R. Vadera and N. Kumar, Sci. Adv. Mater. 2014, 6,1196-1202.
12 X.G. Liu, D.Y. Geng, S. Ma, H. Meng, M. Tong, D.J. Kang and Z.D. Zhang, J. Appl. Phys. 2008, 104, 064319.
13 X.F. Zhang, J.J. Guo and G.W. Qin, Appl. Phys. Lett. 2014, 104, 252404.
14 T. Wang, H.D. Wang, X. Chi, R. Li and J.B. Wang, Carbon 2014,74, 312-318.
15 X.G. Liu, D.Y. Geng, P.J. Shang, H. Meng, F. Yang, B. Li, D.J. Kang and Z.D. Zhang, J. Phys. D: Appl. Phys. 2008, 41, 175006.
16 Y.H. Xu, Q. Liu, Y.J. Zhu, Y.H. Liu, A. Langrock, M.R. Zachariah and C.S. Wang, Nano Lett. 2013, 13, 470-474
17 J.Y. Xiang, J.P. Tu, Y.F. Yuan, X.L. Wang, X.H. Huang and Z.Y. Zeng,

Electrochim. Acta 2009, 54, 1160-1165.
18 X.W. Lou, C.L. Yuan and L.A. Archer, Adv. Mater. 2007, 19, 3328-3330.
19 H. Liu, S. Chen, G.X. Wang and S.Z. Qiao, Chem. Eur. J. 2013, 19, 16897-16901.
20 B. Li, J.T. Zai, Y.L. Xiao, Q.Y. Han and X.F. Qian, CrystEngComm 2014, 16, 3318-3322.
21 J. Xie, J. Yang and X.Y. Zhou, RSC Adv. 2014, 4, 572-577.
22 M. Jagannathan and K.S. Ravi Chandran, J. Power Sources 2014, 247, 667-675.
23 S.L. Jing, F. Gu, J.H. Kong, C.R. Ma, P.S. Lee and C.Z. Li, RSC Adv. 2014, 4, 10450-10453.
24 L. Zhang, H.B. Wu, B. Liu and X.W. Lou, Energy Environ. Sci. 2014, 7, 1013-1017.
25 Y. Zhao, J. Li, N. Wang, C. Wu, G. Dong and L. Guan, J. Phys. Chem. C. 2012, 116, 18612-18617.
26 H.D. Liu, J.M. Huang, C.J. Xiang, J. Liu and X.L. Li, J. Mater. Sci: Mater. Electron. 2013, 24, 3640-3645.
27 Z.B. Fang, J.J. Huang, W.J. He, X.S. Zhang, Y.P. Wu and J.W. Qing, Electrochim. Acta 2013,109, 454-460.
28 X.Y. Xue, Z.H. Chen, L.L. Xing, S. Yuan and Y.J. Chen, Chem. Commun. 2011, 47, 5205-5207.ho
29 L.Y. Beaulieu, K.C. Hewitt, R.L. Turner, A. Bonakdarpour, A.A. Abdo, L. Christensen, K.W. Eberman and J.R. Dahn, J. Electrochem.Soc. 2003, 150, A149-A156.
30 H. Xia, S. Tang and L. Lu, Mater. Res. Bull. 2007, 42, 1301-1309.
31 Z.H. Wang, X. He, X. Wang, Z. Han, D.Y. Geng, Y.L. Zhu and Z.D. Zhang, J. Phys. D: Appl. Phys. 2010, 43, 495404.
32 M. Di Giulio, A Serra, A. Tepore, R. Rella, P. Siciliano and L. Mirenghi, Mater. Sci. Forum 1996, 203, 143-148.
33 W.K. Choi, H.J. Jung and S.K. Koh, J. Vac. Sci. Technol. A 1996, 14, 359-364.
34 Z. Ma, C.T. Cao, Q.F. Liu and J.B. Wang, Chin. Phys. Lett. 2012, 29, 038401.
35 T. Wang, R. Han, G.G. Tan, J.Q. Wei, L. Qiao and F.S. Li, J. Appl. Phys. 2012, 112, 104903.
36 J.P. Li, P. Wu, Y. Ye, H. Wang, Y.M. Zhou, Y.W. Tang and T.H. Lu, CrystEngComm 2014, 16, 517-521.
37 A.K. Rai, L.T. Anh, J. Gim, V. Mathew and J. Kim, Electrochim. Acta 2013, 109, 461-467.
38 L. Zhang, G.Q. Zhang, H.B. Wu, L. Yu and X.W. Lou, Adv. Mater. 2013, 25, 2589-2593.
39 J.S. Chen and X.W. Lou, Small 2013, 9, 1877-1893.
40 F.Y. Cheng, J. Liang, Z.L. Tao and J. Chen, Adv. Mater. 2011, 23, 1695-1715.
41 Y.J. Hong, M.Y. Son and Y.C. Kang, Adv. Mater. 2013, 25, 2279-2283.

Graphical abstract